Available online at www.sciencedirect.com

ScienceDirect

Energy Procedia 114 (2017) 3927 – 3936

Energy Procedia

13th International Conference on Greenhouse Gas Control Technologies, GHGT-13, 14-18 November 2016, Lausanne, Switzerland

Constrained AVO for CO_2 Storage Monitoring at Sleipner

Bastien Dupuy[a], Verónica A.Torres C.[a,b], Amir Ghaderi[a] *, Etor Querendez[a], Milosz Mezyk[a,b]

[a]*SINTEF Petroleum Research*
[b]*Department of Petroleum Enginering and Applied Geophysics, NTNU*

Abstract

A feasibility study of inverting for CO_2 elastic properties using a model based AVO inversion is carried out. We use principal component analysis on a set of PP reflection coefficients to calculate an optimal basis function for the AVO response of the CO_2 plume. The method is applied to the marine seismic data recorded on the CO_2 storage site at Sleipner to map the extent of CO_2 plume, and provide an estimate of the seismic contrast parameters. Appropriate elastic properties and their variabilities are derived from log data, advanced rock physics models, and error propagation analysis. The sensitivity tests show that it is difficult to discriminate between high CO_2 saturations. We finally obtain high-resolution images of impedance contrasts we aim to use as *a priori* constraints for high-resolution tomography after background trend convolution.

Peer-review under responsibility of the organizing committee of GHGT-13.

Keywords: CO_2, Optimal AVO, PCA, imaging constraints, rock physics models, partial and homogeneous saturations

1. Introduction

Underground CO_2 storage is nowadays considered as a viable technique to mitigate the effect of greenhouse gas emissions. At the Sleipner CO_2 storage pilot in the North Sea, 1 million tons of CO_2 per year have been injected since 1996 into the Utsira formation, which is located at an approximate depth of 1000 m. To monitor the behavior of the CO_2 plume in time, 3D seismic surveys have been shot since 1994 making Sleipner a very interesting pilot test to assess safety of such underground storage. In addition to seismic, various other geophysical techniques are

* Corresponding author. *E-mail address: bastien.dupuy@sintef.no, amir.ghaderi@sintef.no*

Peer-review under responsibility of the organizing committee of GHGT-13.
doi:10.1016/j.egypro.2017.03.1524

commonly used for monitoring CO_2 migration in underground storage sites. Chadwick and Eiken [10] give an overview of the different monitoring techniques deployed at Sleipner, with 2D-3D multi-channel marine seismic acquisition, Controlled-Source ElectroMagnetic (CSEM), seabed gravity, being the most prominent ones. From the aforementioned methods, seismic methods are well known to give the highest resolution to track CO_2 plume migration.

The CO_2 is injected to the Utsira formation, which consists of weakly consolidated sandstone with interlayered shale beds. Even if the seismic signature of CO_2 bearing sand layers are clearly visible on migrated data [2], these thin shales layers make the wave propagation complex and consequently the seismic response difficult to interpret quantitatively. They can also be at the origin of complex poroelastic effects due to the supercritical phase of the injected CO_2 [25, 7]. Time-lapse data analysis shows an increase of reflectivity due to the sharp elastic contrasts between overburden shale layers and CO_2-brine saturated sands. Using time-lapse effects like the 4D time-shift and 4D amplitude changes in the pre-stack data from Sleipner, Ghaderi and Landrø [15] introduced an inversion scheme able to simultaneously give a quantitative estimate of the velocity and thickness changes for single thin CO_2-layers. Other qualitative studies have been carried out: Furre et al. [14] derived thickness estimates based on attributes analysis (time shifts and amplitudes) while Williams and Chadwick [31] focus on the thin-layer tuning effect quantification using frequency spectral decomposition method. Several authors [22, 24] applied Full Waveform Inversion (FWI) to derive highly resolved quantitative estimates of wave velocities but were limited by the lack of low frequencies in the data and the limited available offset (maximum offset of 1.8 km).

In this context, Amplitude Versus Offset (AVO) based analysis seems to be a valuable technique for monitoring the CO_2 storage processes [5], even if it is shown that the interpretation is difficult due to tuning effects in thin layers. Ravazzoli and Gomez [23] give an overview of AVO attribute sensitivity as a function CO_2 saturation, effect of thin layer accumulations and the behaviour of the reflectivity as function of saturation, frequency and thickness for normal incidence. Li et al. [19] use the frequency dependent AVO attribute on synthetic data to provide an inversion scheme giving quantitative measure of the dispersion anomalies caused by CO_2. Some preliminary works have also been presented by Buddensiek et al. [6, 9] with a focus on the discrimination of layer thickness effects in the AVO response. Due to the strong tuning effects related to thin interlayers reflections, conventional Zoeppritz-based methods usually fails in such environment. Buddensiek et al. [6] proposed to use constrained AVO inversion, based on the computation of optimal basis functions [8].

This paper will present a systematic study of optimal AVO analysis applied to the Sleipner data. In a first stage, we introduce the data and the methodology of constrained AVO. We then evaluate the sensitivity of optimal AVO attributes to CO_2 saturation on a simple two-layer case. In a third stage, we present and discuss the results of application of the AVO analysis workflow to the selected real data vintage.

2. Data and method

2.1. Seismic dataset: 2D line 2008 vintage

For this study, a 2D dataset has been extracted from the 2008 3D pre-stack time migrated cube. A common processing workflow was derived to process baseline and repeat dataset in order to prepare data for time-lapse studies. The main steps in the processing workflow consist of:

- Low cut filter (6Hz (24dB/oct)
- Deterministic zero-phase conversion using far field signature
- 2 pass swell noise attenuation
- Tidal static and gun and cable static correction
- Gap deconvolution in the Tau-p domain
- Phase, time and amplitude match to baseline survey data
- Data binning to match baseline survey
- Fold normalization using Tau-p interpolation
- Migration velocity analysis

The provided dataset are cropped in time and offset, with a maximum offset of 1900m. The final full offset stack corresponding to the extracted dataset is shown in Fig. 1.

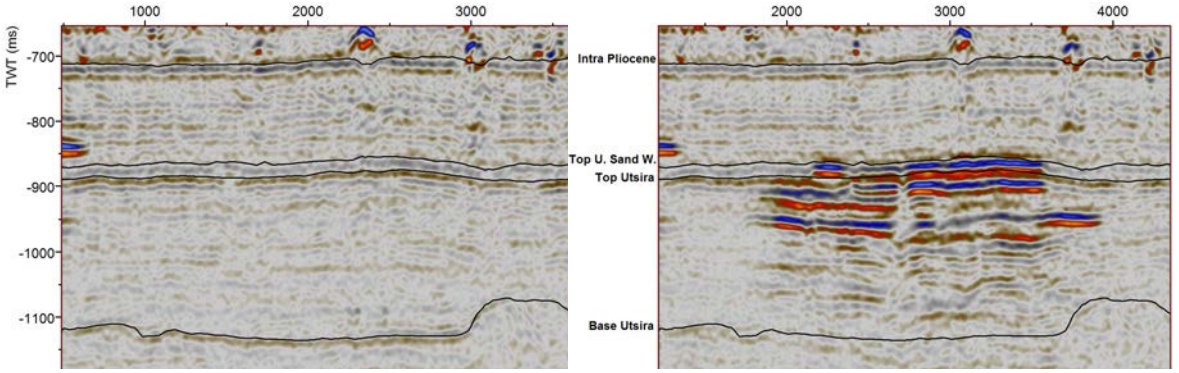

Fig. 1. Inline 1838 crossing the injection point, extracted from (a) the baseline 3D time migrated cubes shot in 1994 and (b) 2008 repeat survey (Courtesy of Statoil).

2.2. Rock physics properties in Sleipner Utsira sandstone derived from log data

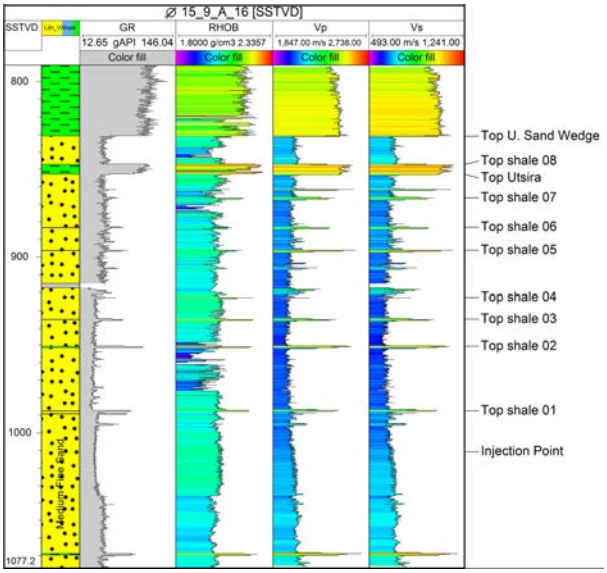

Fig. 2. Logs from the injection well at Utsira. (Courtesy of Statoil). From left to right: Lithology from Vshale, gamma ray, density, sonic P-wave velocity and derived S-wave velocity from [Vernik et al., 2002] relation.

Utsira reservoir formation is a weakly consolidated sandstone located between 800 and 1100 m deep around Sleipner. Even if the sand is quite homogeneous, it contains thin interlayered shales, typically 1 to 2 m thick. The CO_2 is injected in a supercritical state near the bottom of the sand reservoir. Elastic properties of overburden shales, brine-saturated Utsira sand and interlayered shales are derived from sonic and density well log data (injection well, see Fig. 2). The S-wave velocity is calculated from sonic P-wave velocity via the empirical Vernik relation [29]. Computing mean and standard deviations values for each of lithologies (overburden shales, Utsira brine sands and interlayered shales) allow to describe a set of reference models used in the AVO modelling. It is worth mentioning that the potential dispersion of seismic waves between sonic and surface seismic data is neglected. This assumption can be discussed but it is shown that brine saturated sands have a low dispersion in normal settings [20].

While the elastic properties of baseline lithologies (shales and brine sands) and their variabilities are described by log data (see Fig. 2), the elastic properties of sands partially saturated with brine and supercritical CO_2 are calculated using an appropriate rock physics model. As a first order realistic approximation, an effective fluid phase theory is used to compute effective average fluid properties of the mix of supercritical CO_2 and brine. The effective properties (bulk modulus K_f, viscosity η and density ρ_f) of the fluid phase are then plugged into the poroelastic Biot theory [12]. Using this effective fluid phase theory, the assumption is that the saturation is uniform, at least at the seismic scale, i.e. that the fluid gradient equilibrations are the same for both fluid phases (no patches). The bulk density of

the effective fluid ρ_f can be computed with Voigt average [30] with respect to brine saturation S_w, brine density ρ_w, CO_2 saturation S_{CO2} and CO_2 density ρ_{CO2}:

$$\rho_f = S_w \rho_w + S_{CO2} \rho_{CO2}. \quad (1)$$

The effective bulk modulus K_f is derived using the Brie average [4] from brine bulk modulus K_w and CO_2 bulk modulus K_{CO2}, with exponent e equal to 5 [7]:

$$K_f = (K_w - K_{CO2}) S_w^e + K_{CO2}. \quad (2)$$

In accordance with Carcione et al. [7], the effective viscosity η is calculated with Teja and Rice formula [27] from brine viscosity η_w and CO_2 viscosity η_{CO2} as:

$$\eta = \eta_{CO2} \left(\frac{\eta_w}{\eta_{CO2}}\right)^{S_w}. \quad (3)$$

These three effective fluid properties are then combined with rock frame properties using the Biot-Gassmann theory extended with Johnson-Koplik-Dashen (JKD) model [18, 21]. The elastic properties (P-wave velocity V_P, S-wave velocity V_S and bulk density ρ) are expressed as:

$$V_P = \left[Re\left\{ \left(\gamma - \left(\gamma^2 - \frac{4\left(\rho\rho_t - \rho_f^2\right)}{HM - C^2} \right)^{\frac{1}{2}} \right)^{1/2} \right\} \right]^{-1}, \quad (4)$$

$$V_S = \left[Re\left\{ \left(\frac{\rho - \frac{\rho_f^2}{\rho_t}}{G} \right)^{\frac{1}{2}} \right\} \right]^{-1}, \quad (5)$$

$$\rho = (1 - \phi)\rho_s + \phi \rho_f. \quad (6)$$

With γ and H terms:

$$\gamma = \frac{\rho M + \rho_t H - 2\rho_f C}{HM - C^2}, \; H = K_U + \frac{4}{3} G. \quad (7)$$

The velocities are finally expressed with four mechanical terms (undrained bulk modulus K_U, shear modulus G, Biot C modulus and fluid storage term M) and three inertial terms (bulk density ρ, fluid density ρ_f and flow resistance term ρ_t derived in the JKD model). These seven terms are dependent on several microscale properties [11]: grains properties (bulk modulus K_s, shear modulus G_s, density ρ_s), rock frame properties (porosity φ, permeability k_0, dry bulk modulus K_D, dry shear modulus G_D, cementation factor m) and fluids properties (brine bulk modulus K_w, CO_2 bulk modulus K_{CO2}, brine viscosity η_w, CO_2 viscosity η_{CO2}, brine density ρ_w and CO_2 density ρ_{CO2}).

2.3. Constrained AVO analysis

For conventional AVO analysis, the AVO responses are approximated by linear trigonometric functions of offset or angle. These are the linearized approximations, for instance Aki and Richards [1], of the exact expressions of plane-wave reflection coefficients (Zoeppritz equations [32]) to describe amplitude variation with offset curves. These approximations are strictly only valid for small seismic parameter changes across reflectors or small incident angles. Causse et al. [8] present a method for deriving linear AVO approximations from modelled AVO curves. For

this purpose *a priori* information, e.g. from well log data, is integrated to define a most accurate AVO approximation model for the special geological situation of interest. This is a statistical method and the modelled reflection coefficients should contain, and thereby constrain, the natural variability possible in the system. The AVO responses are then modelled for a set of defined reflector classes which are based on prior knowledge of lithologies and their fluid content, and of interfaces. This results in a set of reference curves R(θ) as a function of angle θ. Then singular value decomposition of the reference curves is applied to yield:

$$R(\theta) \approx c_1 f_1(\theta) + c_2 f_2(\theta) + c_3 f_3(\theta) + \ldots \quad (8)$$

In equation (8), f_1, f_2,... are basis functions, and C_1, C_2,... are coefficients parameterizing the equation. The modelled reflection coefficients are computed for different sets of contrast triplets taking into account the level uncertainties in the parameters used. Attributes of the real data are obtained by fitting the prestack amplitudes by least-square fitting to equation (8). The estimated attributes are then calibrated before used for a classification. The calibration is performed in an area of the data where one or several specific classes are expected to be found. A scaling factor is extracted from this area and applied to the attribute sections so that the estimated attributes can be compared with the modelled attributes for classification. In the sensitivity tests of part 3, we compare the results with the well-known Ursin-Dahl approximation [28], describing the PP reflection R(θ) with respect to three AVO attributes (intercept R_0, gradient G and curvature A_3) as:

$$R(\theta) \approx R_0 + G \sin^2\theta + A_3 \sin^2\theta \tan^2\theta. \quad (9)$$

This three "conventional" attributes can be approximated [1] from the elastic velocities V_P and V_S, from the elastic contrasts ΔV_P, ΔV_S and $\Delta\rho$, and from the arithmetic averages V_{Pm}, V_{Sm} and ρ_m as:

$$R_0 = \frac{1}{2}\left(\frac{\Delta V_P}{V_{Pm}} + \frac{\Delta\rho}{\rho_m}\right), \quad (10)$$

$$G = \frac{1}{2}\frac{\Delta V_P}{V_{Pm}} - 2\left(\frac{V_S}{V_P}\right)^2\left(2\frac{\Delta V_S}{V_{Sm}} + \frac{\Delta\rho}{\rho_m}\right), \quad (11)$$

$$A_3 = \frac{1}{2}\frac{\Delta V_P}{V_{Pm}}. \quad (12)$$

Smith and Gidlow [26] proposed another approximation based on impedances contrasts as $I_P = \rho V_P$ and $I_S = \rho V_S$:

$$R(\theta) \approx \left(\frac{1}{2} + \frac{1}{2}\tan^2\theta\right)\frac{\Delta I_P}{I_{Pm}} - 4\frac{V_S^2}{V_P^2}\frac{\Delta I_S}{I_{Sm}}\sin^2\theta + \left(2\frac{V_S^2}{V_P^2}\sin^2\theta - \frac{1}{2}\tan^2\theta\right)\frac{\Delta\rho}{\rho_m}, \quad (13)$$

I_{Pm}, I_{Sm} and ρ_m being the arithmetic averages of the values above and below the interface. These two linearized approximations will be used to convert the AVO attributes in elastic and impedances contrasts for the Sleipner data case.

3. Discrimination of CO_2 saturations using optimal AVO attributes

3.1. Test case and rock physics properties

The Utsira sand reservoir properties are described in Tab. 1 and have been extracted from various authors [13, 3, 14, 16, 15]. As the rock grains are not purely quartz, the effective grains properties are computed with Hashin-Shtrikman formulas [17] taking into account the relative proportions of quartz, calcite, feldspar, albite, aragonite, muscovite and biotite. Each property is given with a relative uncertainty which has been calculated considering the uncertainties in measurements (well data versus lab measurements for example). Due to uncertainties related to

pressure and temperature in the reservoir, the uncertainties related to CO_2 properties are greater than uncertainties on other parameters [15]. An error propagation method is then used to calculate the related uncertainties on P- and S-wave velocities. Fig. 3 gives the elastic properties for different values of CO_2 saturations. P-wave velocity drops down quickly when few percent of CO_2 is replacing the brine and stay relatively constant for CO_2 saturations greater than 50 %. S-wave velocities and bulk density have a linear behavior, V_S increases with S_{CO2} while ρ decreases. The S-wave velocity variations are small as the fluid dependence of V_S is only contained in the density term (shear modulus independent of fluid properties).

Table 1. Utsira sand parameters and brine and CO_2 properties and their associated uncertainties.

Properties	Parameter	Value	Uncertainty
Grain	K_s (GPa)	39.3	3.6
	G_s (GPa)	44.8	1.8
	ρ_s (kg/m^3)	2664	0.1
Frame	K_D (GPa)	2.56	3
	G_D (GPa)	8.5	3
	k_0 (m^2)	2 10^{-12}	75
	m	1	25
	Φ	0.37	6.75
Brine	K_w (GPa)	2.31	3.24
	ρ_w (kg/m^3)	1030	1.94
	η_w (Pa.s)	0.00069	1.5
CO_2	K_{CO2} (GPa)	0.08	53
	ρ_{CO2} (kg/m^3)	700	11
	η_{CO2} (Pa.s)	0.00006	17

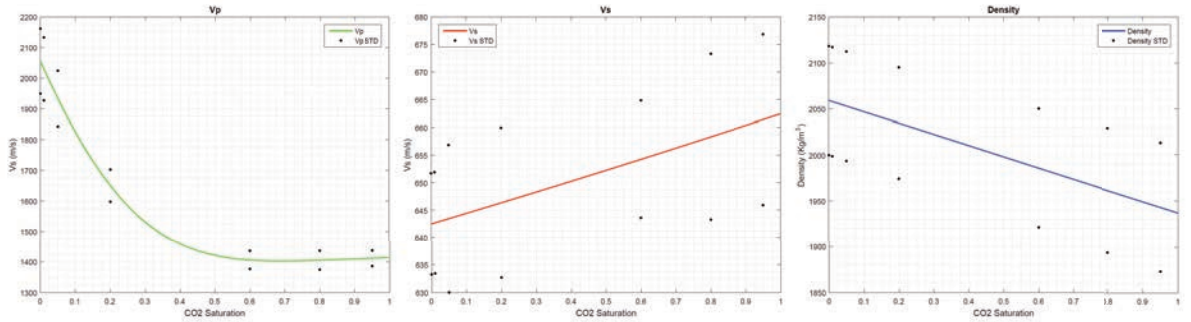

Fig. 3. (a) P-wave velocity V_P, (b) S-wave velocity V_S and (c) density ρ variations with CO_2 saturation. The uncertainty related to 1, 2, 5, 20, 60, 80 and 95 % of CO_2 saturation are given by the black dots.

In order to discriminate between CO_2 saturations in different AVO attributes spaces, we define a simple two-layer model with shales at the top and brine/CO_2 sands at the bottom. We compute the theoretical PP reflection response with Zoeppritz equations [32] and we invert it using Aki-Richards approximation [1] and optimal AVO basis. The AVO models are defined as follow:

- the shales (overburden and intralayer) and brine sands properties are derived from log data (Fig. 2) and the "natural" variability of log data allows to compute elastic properties mean and standard deviation values (as well as correlation between V_P, V_S and ρ).

- The CO_2 sands elastic properties are computed using the rock physics model defined in part 2.2 and taking into account the uncertainties to calculate the associated standard deviation. Four different CO_2 saturation cases are computed: 5, 20, 80 and 95 %.
- For each lithology (shales, brine sands, four CO_2 sands), 25 random models are computed using a Gaussian distribution (based on mean and standard deviation values for each lithology).

3.2. Sensitivity tests for discriminating CO_2 saturations on AVO attributes.

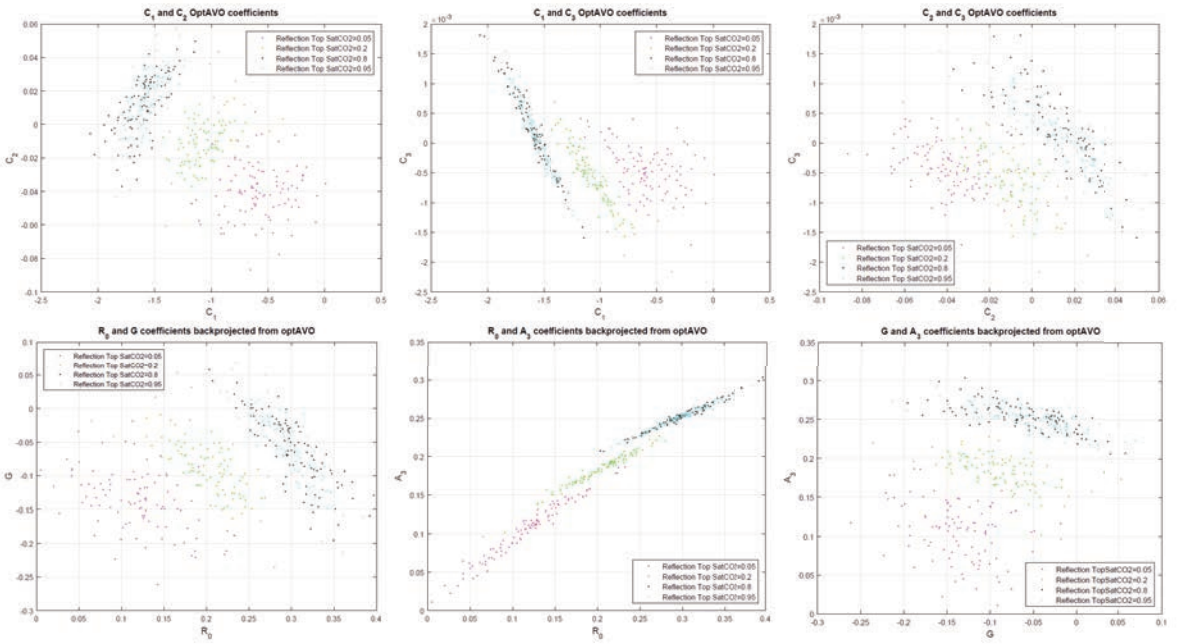

Fig. 5. Crossplots of AVO attributes (optimal AVO coefficients C_1, C_2 and C_3, conventional AVO coefficients R_0 (intercept), G (gradient) and A_3 (curvature)) for a reflection between shales and CO_2 sands with different saturations (5, 20, 80 and 95 %). (a) C_1 vs. C_2, (b) C_1 vs. C_3, (c) C_2 vs. C_3, (d) R_0 vs. G, (e) R_0 vs. A_3 and (f) G vs. A_3.

Fig. 5 show the crossplots of optimal coefficients C_1, C_2 and C_3 and the crossplots of back-projected conventional AVO coefficients R_0, G and A_3 for a simple two layers model with a shale layer above and a CO_2 sand layer below with four different CO_2 saturations. It is easy to discriminate between 5, 20 and 80/95 % saturations on the C_i coefficients crossplots, especially on C_1-C_3 crossplot. 80 and 95 % CO_2 saturation are mixed up. R_0-G crossplot allows also to discriminate between low and high saturations but it is more difficult on R_0-A_3 crossplot. Globally, the optimal AVO coefficients are better for discriminating the CO_2 saturations.

4. AVO analysis of Sleipner data

The PSTM 2008 section (Fig. 1) is inverted using an optimal AVO workflow. The log data (Fig. 2) and the rock physics model are used to define a set of reflections between overburden shales, intralayer shales, brine sands and CO_2-brine sands with various saturations. Three basis functions are computed based on the set of AVO models and the data are fitted with them to derive optimal AVO coefficients C_i (Fig. 6). As the optimal AVO workflow is based on Principal Component Analysis (PCA), the first coefficient C_1 gathers most of the contribution. Second and

especially third coefficients are noisier, which is logical because C_2 and C_3 have less and less contribution. The optimal coefficients are then back-projected in the conventional AVO space (R_0, G, A_3) and calibrated [8]. We see in Fig. 6 that the intercept and gradient coefficients are less noisy than curvature. It is worth noting the strong amplitudes due to CO_2 partial saturation accumulating at the top of Utsira layers.

The AVO attributes are then converted to elastic and impedances contrasts via Ursin and Dahl [28] and Smith and Gidlow [26] approximations (equations 9 and 13). Fig. 7 shows that the impedance contrasts parametrization is better than velocity contrasts parametrization. The P- and S-wave velocity contrasts are of poor quality while P- and S-waves impedance contrasts give a high-resolution quantitative estimation of reflected events.

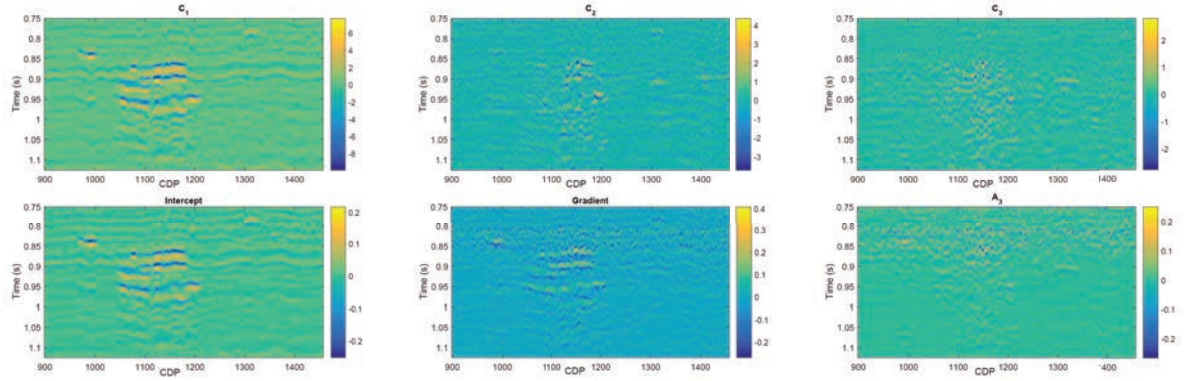

Fig. 6. Optimal AVO attributes derived from Sleipner data. (a) C_1, (b) C_2, (c) C_3, and back-projected conventional AVO attributes (d) R_0, (e) G and (f) A_3.

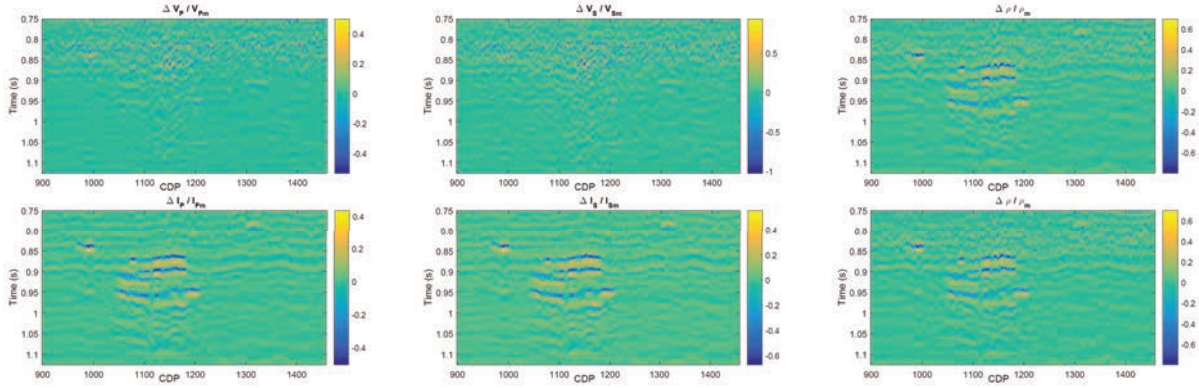

Fig. 7. Elastic and impedance contrasts derived from AVO attributes for Sleipner data. (a) $\Delta V_P/V_{Pm}$, (b) $\Delta V_S/V_{Sm}$, (c) $\Delta\rho/\rho_m$, (d) $\Delta I_P/I_{Pm}$, (e) $\Delta I_S/I_{Sm}$, (f) $\Delta\rho/\rho_m$.

5. Conclusion

Based on log data and advanced rock physics models to define appropriate elastic properties of Utsira and overburden layers, we have tested constrained AVO approach on Sleipner data. First, the sensitivity tests performed on simple two-layer models showed that the discrimination between high CO_2 saturations is not possible. Secondly, the application of the optimal AVO inversion to a PSTM section of 2008 Sleipner dataset show that we are able to

derive high-resolution impedance contrasts through the AVO workflow while elastic contrasts results are of poor quality.

The extension of this work will focus on considering more complex saturation distribution (especially patchy saturation), on determining the best way to take into account the tuning effect of thin layers using synthetic zero-offset reflection response tests and on deriving absolute impedance and elastic properties by convolution with appropriate low frequency background trends. The final goal consists in using the high-resolution absolute elastic properties derived from optimal AVO as *a priori* to constrain high-resolution imaging.

Acknowledgements

This work has been produced with support from the BIGCCS Centre, performed under the Norwegian research program Centers for Environment-friendly Energy Research (FME). The authors acknowledge the following partners for their contributions: ConocoPhillips, Gassco, Shell, Statoil, TOTAL, ENGIE and the Research Council of Norway (193816/S60 and 233716/E20) for their support.

References

[1] K. Aki and P. G. Richards. *Quantitative seismology, theory and methods, second edition*. University Science Books, Sausalito,California, 2002.

[2] R. Arts, O. Eiken, A. Chadwick, P. Zweigel, L. van der Meer, and B. Zinszner. Monitoring of CO_2 injected at sleipner using time-lapse seismic data. *Energy*, 29:1383 – 1392, 2004. 6th International Conference on Greenhouse Gas Control Technologies.

[3] Fran Boait, Nicky White, Andy Chadwick, David Noy, and Mike Bickle. Layer spreading and dimming within the CO_2 plume at the sleipner field in the North Sea. *Energy Procedia*, 4:3254 – 3261, 2011.

[4] A. Brie, F. Pampuri, A.F. Marsala, and O. Meazza. Shear sonic interpretation in gas-bearing sands. *SPE Annual Technical Conf. 30595*, pages 701–710, 1995.

[5] Stephen Brown, Gilles Bussod, and Paul Hagin. AVO monitoring of CO_2 sequestration: A benchtop-modeling study. *The Leading Edge*, 26(12):1576–1583, 2007.

[6] M. L. Buddensiek, S. Sturton, and M. Dillen. AVO analysis of thin layers - Applications to CO_2 storage at Sleipner. In *72nd EAGE Conference and Exhibition incorporating SPE EUROPEC 2010*, 2010.

[7] J.M. Carcione, S. Picotti, D. Gei, and G. Rossi. Physics and seismic modeling for monitoring CO_2 storage. *Pure and Applied Geophysics*, 163:175–207, 2006.

[8] E. Causse, M. Riede, A. J. van Wijngaarden, A. Buland, J. F. Dutzer, and R. Fillon. Amplitude analysis with an optimal model-based linear AVO approximation: Part I - Theory. *Geophysics*, 72(3):C59–C69, 2007.

[9] Andy Chadwick, Gareth Williams, Nicolas Delepine, Vincent Clochard, Karine Labat, Susan Sturton, Maike-L Buddensiek, Menno Dillen, Michael Nickel, Anne-Louise Lima, Rob Arts, Filip Neele, and Giuliana Rossi. Quantitative analysis of time-lapse seismic monitoring data at the Sleipner CO_2 storage operation. *The Leading Edge*, 29(2):170–177, 2010.

[10] RA Chadwick and O Eiken. Offshore CO_2 storage: Sleipner natural gas field beneath the North Sea. *Geological Storage of Carbon Dioxide (CO_2): Geoscience, Technologies, Environmental Aspects and Legal Frameworks, Woodhead Publishing*, pages 227–250, 2013.

[11] B. Dupuy, L. De Barros, S. Garambois, and J. Virieux. Wave propagation in heterogeneous porous media formulated in the frequency-space domain using a discontinuous Galerkin method. *Geophysics*, 76(4):N13–N28, 2011.

[12] B. Dupuy and A. Stovas. Influence of frequency and saturation on AVO attributes for patchy saturated rocks. *Geophysics*, 79(1):B19–B36, 2014.

[13] Anne-Kari Furre and Ola Eiken. Dual sensor streamer technology used in sleipner co2 injection monitoring. *Geophysical Prospecting*, 62(5):1075–1088, 2014.

[14] Anne-Kari Furre, Anders Kiær, and Ola Eiken. CO_2-induced seismic time shifts at Sleipner. *Interpretation*, 3(3):SS23–SS35, 2015.

[15] Amir Ghaderi and Martin Landrø. Estimation of thickness and velocity changes of injected carbon dioxide layers from prestack time-lapse seismic data. *Geophysics*, 74(2):O17–O28, 2009.

[16] William G. Gray, Paulo A. Herrera, Sarah E. Gasda, and Helge K. Dahle. Derivation of vertical equilibrium models for CO_2 migration from pore scale equations. *International Journal of Numerical Analysis and Modeling*, 9(3):745–776, 2012.

[17] Z. Hashin and S. Shtrikman. A variational approach to the elastic behavior of multiphase materials. *Journal of the Mechanics and Physics of Solids*, 11:127–140, 1963.

[18] D.L. Johnson, J. Koplik, and R. Dashen. Theory of dynamic permeability and tortuosity in fluid-saturated porous media. *Journal of Fluid Mechanics.*, 176:379–402, 1987.

[19] Bonan Li, Cai Liu, Qi Lu, and Shuo Pang. Modeling CO_2 vertical migration based on seismic frequency-dependent AVO responses. *Journal of Geophysics and Engineering*, 13:164–171, 2016.

[20] T.M. Muller, B. Gurevich, and M. Lebedev. Seismic wave attenuation and dispersion resulting from wave-induced flow in porous rocks - A review. *Geophysics*, 75(5):147–164, 2010.

[21] S.R. Pride. *Hydrogeophysics*, pages 253–284. Water Science and Technology Library, Springer, The Netherlands, 2005.
[22] Manuel QueiBer and Satish C. Singh. Full waveform inversion in the time lapse mode applied to CO_2 storage at Sleipner. *Geophysical Prospecting*, 61(3):537–555, May 2013.
[23] Claudia Ravazzoli and Julian Gomez. *CO_2 sequestration and valorization*, chapter Seismic reflectivity in carbon dioxide accumulations: A review. InTech, 2014.
[24] Anouar Romdhane and Etor Querendez. CO_2 characterization at the Sleipner field with full waveform inversion: application to synthetic and real data. *Energy Procedia*, 63:4358–4365, 2014.
[25] J. G. Rubino, D. R. Velis, and M. D. Sacchi. Numerical analysis of wave-induced fluid flow effects on seismic data: Application to monitoring of CO_2 storage at the Sleipner field. *Journal of Geophysical Research*, 116, 2011.
[26] G. C. Smith and P. M. Gidlow. Weighted stacking for rock property estimation and detection of gas. *Geophysical Prospecting*, 35:993–1014, 1987.
[27] A.S. Teja and P. Rice. Generalized corresponding states method for viscosities of liquid mixtures. *Industrial and Engineering Chemistry Fundamentals*, 20:77–81, 1981.
[28] B. Ursin and T. Dahl. Seismic reflection amplitudes. *Geophysical Prospecting*, 40:483–512, 1992.
[29] L. Vernik, D. Fisher, and S. Bahret. Estimation of net-to-gross from P and S impedance in deepwater turbidites. *The Leading Edge*, 21:380–387, 2002.
[30] W. Voigt. Uber die beziehung zwischen den beiden elastizitatkonstanten isotroper körper. *Annalen der Physik*, 38:573–587, 1889.
[31] Gareth Williams and Andrew Chadwick. Quantitative seismic analysis of a thin layer of CO_2 in the sleipner injection plume. *GEOPHYSICS*, 77(6):R245–R256, 2012.
[32] K. Zoeppritz. Über Reflexion und Durchgang seismischer Wellen durch Unstetigkeitsflächen, über Erdbebenwellen VIIb. *Nachrichten von der Königlichen Gesellschaft der Wissenscaften zu Göttingen, Mathematisch-Physikalische Klasse*, KI:66–84, 1919.